Indian Journal of Experimental Biology
Vol. 64, November 2026, 1079-1090
DOI: 10.56042/ijeb.v64i11.26116

Hydrocotyle javanica Thunb and chitosan functionalized zinc oxide nanocomposites for enhanced antioxidant and antibacterial applications

Anjini Bellai & Pallabi Kalita Hui*

Phytochemistry Lab, Department of Biotechnology, National Institute of Technology, Jote, 791 113, Arunachal Pradesh, India

Received 9 December 2025; *revised 03 August 2026*

Plant-mediated nanoparticle synthesis has gained attention due to the growing demand for eco– friendly and biocompatible materials. *Hydrocotyle javanica* (*H. javanica*), an ethnomedicinal herb rich in flavonoids, phenolics, and sesquiterpenes, remains underexplored for such applications. This study reports the green synthesis of zinc oxide nanoparticles (ZnO NPs) using *H. javanica* extract coated with chitosan (ZnO-HJ-CS), which was characterized through XRD, FTIR, zeta potential and particle size distribution (PSD), and subsequently evaluated for antioxidant (DPPH, SOD, NOD and OH assays) and antimicrobial activities (against *E. coli*, *S. aureus*, *S. pneumoniae*, *S. epidermidis*, and *B. subtilis*). XRD analysis of ZnO-HJ-CS demonstrated a hexagonal wurzite structure, consistent with the ZnO standard reference (JCPDS No. 01-079-2205). FTIR spectra exhibited broadening and shifting of peaks along the O-H, C=C, and C-O str*etc*hes. SEM analysis revealed an irregular, roughened surface morphology. Compared to pure ZnO, the PSD shifted to 702 nm, with a zeta potential of -15.1 mV. ZnO-HJ-CS exhibited antioxidant activity with IC_{50} values of 34.3, 74.5, 27.3 and 63.6 µg/mL in the respective assay, while exhibiting pronounced antibacterial activity against *E. coli* (IC_{50} values of 53.31 µg/mL) and *S. aureus* (57.52 µg/mL) among all the tested bacterial strains.

Keywords: Disc diffusion, Green synthesis, Macro broth dilution, Particle size distribution, Zinc oxide nanoparticles

Nanotechnology has significantly reshaped the domain of biomedical sciences by enabling precise manipulation at the nanoscale for drug delivery, diagnostics, and therapeutic development[1]. Metal oxide nanoparticles continue to draw substantial interest due to their structural robustness and high surface reactivity physicochemical features[2]. ZnO NPs have been extensively studied for its antimicrobial potential, ultraviolet (UV) blocking capacity, and semiconductor characteristics[3]. ZnO is also listed under the "generally recognized as safe" category by the U.S. Food and Drug Administration (FDA), adding regulatory appeal for its translational use in biomedical platforms[4]. Despite the established benefits of ZnO NPs, their conventional synthesis routes, such as chemical precipitation, hydrothermal treatment, sol-gel methods *etc*., often require harsh reagents, elevated temperatures, and generate toxic effluents[3]. In response, plant-mediated synthesis is particularly attractive due to its rich repository of natural metabolites that function as intrinsic reducing, capping, and stabilizing agents[4]. Among the medicinal plants explored for green synthesis, *H. javanica* *remains* largely underutilized despite its considerable phytochemical composition and pharmacological potential[5].

H. javanica, a creeping herbaceous species in the Araliaceae family, is native to the tropical and subtropical regions of Southeast Asia, including northeastern India, China, Bhutan, and Thailand[6].

Traditionally it has been used for treating digestive disorders, skin infections, neurological conditions *etc*[7]. Phytoconstituent analysis of *H. javanica* has revealed the presence of phenolic acids, flavonoids, tannins, and glycosides, all of which are known for their redox-modulating, antimicrobial and anti-oxidant properties[8,9].

Incorporating chitosan into nanoparticle systems has gained substantial attention for addressing challenges related to colloidal instability and suboptimal bioavailability[10]. Chitosan enhances antimicrobial and drug delivery performance by interacting with negatively charged bacterial membranes, causing membrane damage and biofilm disruption[11]. When used in tandem with green-synthesized metal oxide nanoparticles, chitosan coatings may promote a synergistic enhancement in biological efficacy, particularly by augmenting antimicrobial potency and facilitating controlled therapeutic release[12]. Recent

*Correspondence:
E-mail: pallabikalita@nitap.ac.in

advances have demonstrated the promise of chitosan-coated ZnO NPs and plant-mediated ZnO NPs independently, but no studies have explored their integration using *H. javanica* as the botanical precursor[13]. This represents a clear knowledge gap in developing tri-component systems that combine the intrinsic bioactivities of phytochemicals, the antimicrobial properties of ZnO, and the stabilizing capabilities of chitosan.

This study aims to develop and characterize a ZnO composite functionalized with *H. javanica* and chitosan using a green synthesis method. The antioxidant and antibacterial activities of the synthesized composites was systematically evaluated. Additionally, nutritional and mineral profiling of *H. Javanica* was also undertaken.

Materials and Methods

Collection and preparation of sample

Fresh sample of *H. javanica* was collected from Goiliang circle, Anjaw District, Arunachal Pradesh, India during the month of October, 2024. The sample was identified and the voucher specimen was submitted to the Botany Department, Rajiv Gandhi University Arunachal Pradesh under voucher specimen No. HAU/AN-3904. The fresh samples were dried at 20-25°C for overnight. The following day, residual moisture was removed by further drying at 40°C for 2-3 h. Then it was grounded to a fine powder using a mixer grinder, and the resulting powdered sample was stored in an airtight container.

Proximate and Mineral Analysis

The proximate composition of powdered *H. javanica* was analysed following Indian standard (IS) methods established by the Bureau of Indian Standards. Specifically, crude protein content was determined using IS 7219, crude fat using IS 1011, and crude fiber content *via* IS 10226 protocols. These assessments were conducted on a dry weight basis using 100 g of the plant powder to evaluate its macronutrient profile. For mineral analysis, procedures were carried out as per guidelines outlined in the Food Safety and Standards Authority of India Laboratory Manual 9, in conjunction with IS12473 (Part 2 and Part 3). Essential minerals, including calcium, iron, copper, manganese, magnesium, and heavy metals such as cadmium, lead, and nickel were quantified using atomic absorption spectroscopy after appropriate digestion and dilution steps. The concentrations were reported in mg/100 g of dry sample[14].

Extract preparation

Powdered *H. javanica* was extracted with methanol for 24 h, followed by filtration and evaporation under reduced pressure using a rotary vacuum evaporator. Subsequently, the resulting methanolic crude extract of *H. javanica* was collected in a sample storage vial and designated as MEHJ. Subsequently, 2 g of MEHJ mixture was dissolved in 20 mL of distilled water and stirred for 20-30 min until a homogenous solution and filtered under vacuum through Whatman filter paper to obtain MEHJF1 filtrate specifically because the downstream ZnO precipitation reaction required an aqueous-compatible phytochemical carrier.

Synthesis of ZnO NPs coated with MEHJ

The direct precipitation method was employed for the synthesis of ZnO NPs and their composite with *H. javanica* and chitosan, following the protocol described by Abinash *et al*. (2023)[15] with minor modifications. Briefly, 6.5 g of $Zn(NO3)_2.6H_2O$ was dissolved in 100 mL of distilled water and stirred at 500-600 rpm until a homogeneous solution. MEHJF1 was then slowly added to the $Zn(NO3)_2.6H_2O$ homogenous solution under continuous stirring at 500-600 rpm for 20-30 min. Subsequenlty, 0.5 M NaOH was added dropwise to the $Zn(NO3)_2.6H_2O$-MEHJF1 mixture at 45°C, and the Ph of the solution was adjusted to 8. The resulting mixture was stirred at 500-600 rpm for 5-6 h. Thereafter, the mixture was filtered under vacuum suction through Whatman No.1 filter paper. The obtained residue, consisting of ZnO coated with MEHJF1, was transferred to a clean petri dish and dried at 40-50°C for 12 h. After drying, the residue was collected, grounded into a fine powder, transferred to a clean vial, stored in a desiccator, and designated as ZnO-HJ. Pure ZnO NPs were prepared following the same protocol, but without the addition of MEHJF1.

Preparation of chitosan solution

A solution of chitosan (0.1 g) was prepared in a mixture solution of glacial acetic acid and distilled water (1:9 *v/v*). The mixture was sonicated at 35-45 kHz for a few min, and 10 mL of it was transferred to a clean 20 mL beaker. Subsequently, 0.1 g of chitosan was slowly added to the mixture

under continuous stirring at 500-600 rpm and allowed to stir overnight.

Synthesis of ZnO-HJ-CS composite

0.9 gram of ZnO-HJ was dissolved in 4 mL of ethanol and mixed thoroughly under continuous stirring at 500-600 rpm for 30 min. Next, 150 µL of chitosan was added dropwise to the mixture, which was then stirred for an additional 12 h. After 12 h, the ethanol was evaporated under reduce pressure using a rotary vacuum evaporator. Once the mixture was completely dry, it was grounded into a fine powder using a mortar and pestle. The resulting powder was scraped put, transferred to a clean vial, stored, and designated as ZnO-HJ-CS.

Characterisation of Synthesized ZnO-HJ-CS Composite

Comprehensive Characterisation of the synthesized ZnO-HJ-CS composite was performed using a range of analytical techniques to evaluate its structural, morphological, surface charge, and particle size attributes. The employed instruments and methods include FTIR, XRD, scanning electron microscopy (SEM), DLS, and zeta potential analysis.

FTIR spectra of the ZnO-HJ-CS were acquired using a PerkinElmer Spectrum Two FTIR spectrometer equipped with an attenuated total reflectance (ATR) accessory. Samples were directly applied onto the ATR crystal, and spectral scanning was carried out across a wavelength range of 4000–400 cm^{-1} [16].

The crystalline phase composition and structural features of ZnO-HJ-CS were investigated using a Rigaku Smart Lab high-resolution multipurpose X-ray diffractometer. The system was calibrated with a silicon standard and operated under Cu Kα radiation (λ = 1.5405 Å) in Bragg-Brentano geometry mode. XRD data acquisition was performed over a 2θ range of 5°-100° at a rated tube voltage of 30-40 kV and current of 20-40 mA. The obtained diffraction peaks were analysed using XPert HighScore software, and phase identification was validated by matching experimental 2θ values with standard patterns from the JCPDS database[17].

Surface morphology of the ZnO-HJ-CS were examined using a ZEISS EVO-MA10 scanning electron microscope. Prior to imaging, samples were mounted on carbon tape, and sputter-coated with a thin layer of gold to enhance electron conductivity. SEM micrographs were captured at varying magnifications to assess particle shape, dispersion uniformity, and agglomeration tendencies[18].

Surface charge and colloidal stability of the ZnO-HJ-CS were measured using a Zetasizer Nano ZS (Malvern Instruments Ltd., UK). A 0.1 g sample was suspended in distilled water and ultrasonicated for 5 min to obtain a uniform dispersion. The measurement parameters were standardized as follows: temperature at 25 °C, viscosity 0.8872 cP, dispersant refractive index 1.330, dielectric constant 78.5, and count rate of 229.2 kcps. The measurement was conducted with 10 zeta runs, and the analysis position was set at 2.00 mm[19].

The hydrodynamic PSD was determined using DLS with the same instrument setup (Zetasizer Nano ZS). A homogeneous suspension was prepared by dispersing the composite in distilled water and sonicated for 5 min. A disposable polystyrene cuvette was used for the measurement. The parameters were adjusted as follows: dispersant refractive index of 1.330, viscosity 0.8872 cP, and material refractive index of 1.59. Measurements were conducted at 25°C with a positioning depth of 4.65 mm. A 12 mm DTS0012 cell was filled with 1 mL of distilled water, and 50 µL of the stock dispersion was added, followed by brief sonication. The resulting count rate was recorded at 255.8 kcps, and the intercept value was 0.980[20].

Antioxidant Activity

The antioxidant activity of ZnO-HJ-CS was systematically evaluated using four established radical scavenging assays: 2,2-diphenyl-1-picrylhydrazyl (DPPH), nitric oxide dismutase (NOD), superoxide Dismutase (SOD), and hydroxyl (OH) radical scavenging. Each assay was performed in comparison with a standard antioxidant, either gallic acid or ascorbic acid. For all assays, a stock solution of ZnO-HJ-CS at a concentration of 1 mg/mL was prepared, and working concentrations were diluted to a range of 20-100 µg/mL. The percentage inhibition was calculated using the standard formula:

$$\%\ \text{Inhibition of radical} = \frac{Absorbance\ of control - absorbance\ of sample}{Absorbance\ of control} \times 100$$

DPPH scavenging assay

The DPPH assay was employed to assess the free radical scavenging capacity of ZnO-HJ-CS. A 0.2 mM DPPH solution was prepared in methanol. To 2 mL of sample (ZnO-HJ-CS / ascorbic acid at varying

concentrations), 1 mL of DPPH solution was added. The mixture was incubated in the dark at 20-25°C for 30 min. After incubation, the absorbance was recorded at 514 nm using a UV-Visible spectrophotometer. Methanol served as the blank and the control consisted of the sample without test sample[21].

SOD scavenging assay

SOD activity was assessed based on the method involving nicotinamide adenine dinucleotide hydrogen (NADH) mediated reduction of nitroblue tetrazolium (NBT) in the presence of phenazine methosulfate (PMS). The reaction mixture consisted of 3.0 mL Tris-HCl buffer (16 mM, pH 8.0), 0.5 mL of NBT (0.3 mM), 0.5 mL NADH (0.936 mM), 1.0 mL of ZnO-HJ-CS or gallic acid, and 0.5 mL of Tris-HCl buffer. The reaction was initiated by adding 0.5 mL PMS (0.12 mM). After incubation at 25 °C for 5 min, absorbance was recorded at 560 nm. The decrease in absorbance indicated super oxide radical antioxidant activity[22].

NOD scavenging assay

The nitric oxide radical scavenging activity was determined by incubating 0.5 mL of ZnO-HJ-CS or gallic acid solution with 2 mL of 10 mM sodium nitroprusside and 0.5 mL phosphate-buffered saline (PBS, pH 7.4). The reaction mixture was incubated at 25 °C for 150 min. After incubation, 0.5 mL of the resulting mixture was combined with 0.5 mL of Griess reagent and incubated again for 30 min at 25 °C. The absorbance was measured at 546 nm using a UV-Visible spectrophotometer. The decrease in absorbance corresponded to nitric oxide radical scavenging efficacy[23].

OH scavenging assay

Hydroxyl radical scavenging activity was evaluated through the degradation of 2-deoxy-2-ribose by hydroxyl radicals generated in the Fenton reaction system. The reaction mixture comprised 0.5 mL of ZnO-HJ-CS or gallic acid (20-100 µg/mL), 0.1 mL of 0.028 M 2-deoxy-2-ribose, 0.2 mL of 1% $FeCl_3$, 0.1 mL of 0.01 M H_2O_2, and 0.1 mL of 0.01 M EDTA, all prepared in 0.2 M PBS (pH 7.4). The solution was incubated at 37 °C for 1 hour. Following this, 1.0 mL of 1% thiobarbituric acid (TBA) and 1.0 mL of 2.8% trichloroacetic acid (TCA) were added, and the mixture was incubated in a boiling water bath at 100 °C for 20 min. The samples were cooled, and absorbance was measured at 532 nm. Inhibition of TBARS formation indicated OH• scavenging[24].

Antibacterial activity

Bacterial Strains

The bacterial strains used in this study were procured from the Microbial Type Culture Collection and Gene Bank (MTCC), Council of Scientific and Industrial Research-Institute of Microbial Technology (CSIR-IMTECH), Chandigarh, India. The obtained bacterial strains are *Staphylococcus epidermidis* (MTCC 2639), *Staphylococcus aureus* (MTCC 3160), *Streptococcus pneumoniae* (MTCC 1935), *Escherichia coli* (EC 40), and *Bacillus subtilis* (MTCC 1134). All strains were handled aseptically under biosafety conditions appropriate for Biosafety Level 2 organisms.

Inoculum preparation

The bacterial strains were initially cultured in Mueller Hinton Broth (MHB) and incubated in a rotary shaker incubator at 37°C for 24 h. The incubated cultures were then streaked onto Mueller Hinton Agar (MHA) plates and incubated at 37°C for 24 h. Post incubation, the plates were preserved at −20 °C as stock cultures.

Broth microdilution assay

A loopful of each stock culture was inoculated into 10 mL of fresh MHB and incubated at 37°C for 24 h. The turbidity of the bacterial suspensions was adjusted to match the 0.5 McFarland standard and subsequently diluted 1:150 with sterile MHB to achieve approximately 1×10^6 CFU/mL. Standardization was confirmed by measuring the optical density (OD) at 600 nm.

Aliquots of 200 µL of the bacterial suspensions were transferred into 96 well-plates, followed by the addition of 100 µL of ZnO-HJ-CS at varying concentrations ranging from 20 -100 µg/mL. The mixture was incubated at 37°C for 24 h. Absorbance reading was recorded spectro photometrically (Thermo Scientific UV-Visible spectrophotometer) at 600 nm, after which incubation was continued for another 24 h. The same protocol was repeated using *H. javanica.* The MIC was defined as the lowest concentration of the test substance that inhibited visible bacterial growth. The inhibitory concentration 50 (IC_{50}) values were determined by plotting concentration against percentage inhibition curves. All tests were performed in triplicate to ensure statistical validation[25].

Disk diffusion assay

The standard disk diffusion method was employed to determine the zone of inhibition, according to CLSI

guidelines. A 500 µL aliquot of the bacterial suspension was uniformly spread onto the agar surface using a sterile swab. Sterile paper disk was soaked in the standard drug solution and ZnO-HJ-CS solutions at varying concentrations ranging from 20 to 100vµg/mL and then placed onto the inoculated agar plates. The plates were sealed tightly with parafilm and incubated at 37°C for 24 h. After 24 h of incubation zone of inhibition was measured and recorded.

Statistical analysis

Experimental data were expressed as mean ± standard deviation (SD) from three independent replicates (n = 3). The IC_{50} values were determined by applying linear regression analysis to dose–response curves derived from antioxidant and antibacterial assays.

Results

Proximate and mineral composition

The proximate composition of *H. javanica* exhibited a dominant presence of carbohydrates at 72.32 g/100 g, followed by fiber content at 14.12 g/ 100 g, crude fat content at 1.74 g/100 g and protein content at 0.20 g/100 g (Table 1).

The quantitative evaluation of mineral composition in *H. javanica* revealed a notably high calcium concentration (2405.73 mg/100 g), followed by Magnesium (215.63 mg/100 g), Iron content (27.75 mg/100 g), Manganese (10.29 mg/100 g), and copper (4.31 mg/100 g). The concentrations of lead and nickel were found to be below the detection limit, and cadmium was quantified at only 0.41 mg/100 g (Table 2).

Characterisation of Synthesized ZnO-HJ-CS composite

XRD Analysis

The reflections corresponding to the 100), (002), (101), (110), and (201) crystallographic planes of ZnO (JCPDS No.01-079-2205) were observed at 2θ values of 32.01253°, 34.69896°, 36.51506°, 56.82099, and 69.24922°, respectively for ZnO and 32.01255, 34.69895°, 36.51511°, 56.82095°, and 69.24911, respectively, for ZnO-HJ-CS composite, confirming close correspondence between two systems across all indexed planes (Table 3). The full width at half maximum (FWHM) values for these respective planes were 0.4927°, 0.54546°, 0.554°, 0.53152, and 0.36437 for both ZnO and the composite, indicating negligible peak broadening differences between the two. The average crystallite size, calculated for each plane was consistently 14.93 nm for ZnO and 14.8 nm for the composite reflecting marginal reduction in crystallite dimensions upon composite formation. Additionally, the interplanar spacing for the (100), (002), (101), (110), and (201) planes were 0.212404419, 0.229702908, 0.241326221, 0.366497438, and 0.437682342 for ZnO and 0.212404549, 0.229702844, 0.24132654, 0.366497202, and 0.437681734 for composite. Further, the calculated lattice parameters for both

Table 1 — Nutritional composition of *H. javanica*. The parameters shown are common nutritional components measured per 100 grams of the sample

S. No	Test parameters	Results
1	Crude protein	0.20 g/100 g
2	Crude fat	1.74 g/ 100 g
3	Crude fiber	14.12 g/100 g
4	Carbohydrate	72.32 g/ 100 g

Table 2 — Mineral analysis for *H. javanica.* The concentration of various essential and toxic elements per 100 grams of *H. javanica*.

S. No	Test parameters	Results
1	Calcium	2405.73 mg/ 100g
2	Iron	27.75 mg/ 100 g
3	Cadmium	0.41 mg/ 100 g
4	Lead	Below the detection limit
5	Copper	4.31 mg/ 100 g
6	Manganese	10.29 mg/ 100 g
7	Magnesium	215.63 mg/ 100 g
8	Nickel	Below the detection limit

Table 3 — XRD peak characteristics and crystallographic orientations of pure ZnO and ZnO-HJ-CS composite. Average crystal size was calculated using Scherrer equation.

JCPDS N0. 01–079–2205 planer direction (hkl)	XRD peak positions (2θ values in degree)		FWHM		Average crystal size		Interplaner distance ($d = \frac{\lambda}{2sin\theta/2}$)	
	ZnO	ZnO-HJ-CS	ZnO	ZnO-HJ-CS	ZnO	ZnO-HJ-CS	ZnO	ZnO-HJ-CS
(100)	32.01253	32.01255	0.4927	0.4927	14.93	14.8	0.212404419	0.212404549
(002)	34.69896	34.69895	0.54546	0.54546			0.229702908	0.229702844
(101)	36.51506	36.51511	0.554	0.554			0.241326221	0.24132654
(110)	56.82099	56.82095	0.53152	0.53152			0.366497438	0.366497202
(201)	69.24922	69.24911	0.36437	0.36437			0.437682342	0.437681734

Table 4 — Lattice parameters of ZnO-HJ-CS composite in comparison with standard JCPDS values.

Lattice constant	Standard values (Å)	Our calculated values (Å)
a=b	3.2501	3.21
c	5.2071	5.2

ZnO and composite were a = b = 3.21 Å and c = 5.2 Å, which align closely with standard JCPDS values (a = b = 3.2501 Å, c = 5.2071 Å) (Table 4).

FTIR analysis

The FTIR analysis was conducted in the spectral range of 4000-400 cm^{-1}, as illustrated in (Fig. 1b). Compared to the ZnO spectrum (green), the spectrum of the ZnO-HJ-CS composite (blue line), exhibited shifts in peaks from 3450 to 3471 cm^{-1}, 1616 to 1586 cm^{-1}, 1000 to 1038 cm^{-1}, 883 to 892 cm^{-1}, and 630 to 641 cm^{-1}, indicating effective surface modification. The FTIR peaks corresponding to functional groups is presented in (Table 5).

SEM analysis

The SEM image of ZnO demonstrated a hexagonal crystal morphology with defined facets, and smooth surfaces (Fig. 1c), whereas, the SEM image of the ZnO-HJ-CS demonstrated an irregular, rough surface, indicating the successful surface modification of ZnO by coating with *H. javanica* and Chitosan (Fig. 1d).

Zeta potential analysis

The zeta potential measurement of the ZnO-HJ-CS is illustrated in (Fig. 1e), with the corresponding data presented in (Table 6). Pure ZnO exhibited a zeta potential of +15 mV, which shifted to -15.1 mV in the case of the ZnO-HJ-CS composite.

PSD

The DLS analysis showed a pure ZnO peak at 820.2 nm, which shifted to 702.3 nm in case of the ZnO-HJ-CS (Table 7). The graphical representation is illustrated in (Fig. 1f).

***In vitro* antioxidant activity**

ZnO-HJ-CS exhibited dose-dependent radical scavenging activity comparable to the standard antioxidant ascorbic acid and gallic acid (Fig. 2a–d). ZnO-HJ-CS showed DPPH radical inhibition with an IC_{50} of 34.3 ± 0.0031 µg/mL, compared to 10.2 ± 0.008 µg/mL for Ascorbic acid, nitric oxide inhibition with an IC_{50} value of 27.3 ± 0.04 µg/mL, compared to 16.12 ± 0.03 µg/mL for Gallic acid, superoxide inhibition with an IC_{50} of 74.5 ± 0.03 µg/mL, compared to 42.6 ± 0.02 µg/mL for Gallic acid; and hydroxyl radical inhibition with an IC_{50} of 63.6 ± 0.03 µg/mL, which was less potent than Gallic acid (38.7 ± 0.02 µg/mL) (Table 8).

Anti–bacterial activity

MEHJ exhibited higher inhibition against *S. pneumoniae*, with IC_{50} values of 63.9µg/mL at 24 h incubation and 44.41µg/mL after extended incubation for 48 h, followed by *S. aureus* and *E. coli*. Conversely, *B. subtilis* exhibited the highest resistance with an IC_{50} of 99.2 µg/mL at 48 h (Table 9). Lower turbidity of bacterial growth was observed at 80 µg/mL for most strains after 24 h, while by 48 h, growth inhibition was more consistent at 100 µg/mL (Table 10)

ZnO-HJ-CS exhibited higher inhibition against *E. coli,* with IC_{50} values of 53.7µg/mL at 24 h and 53.31 µg/mL at 48 h, followed by *S. aureus* with IC_{50} values of 49.81 µg/mL at 24 h and 57.52 at 48 h. The IC_{50} values and % inhibition of bacterial growth exhibited by ZnO-HJ-CS is summarised in (Table 11). The MIC values of ZnO-HJ-CS was observed at 40 µg/mL at 24 h incubation, increasing to 60 µg/mL at 48 h incubation. The MIC values are summarised in (Table 12). The graphical representation of bacterial growth is presented in (Fig. 3a & b). Additionally, the zone of inhibition exhibited by ZnO-HJ-CS composite against tested bacterial strains is presented in (Table 13), and its images are illustrated in (Figure 4a-e).

Discussion

Nanotechnology, an advanced scientific domain has driven the progress of metal oxide nanoparticles, which provides notable advantages compared to conventional physical and chemical methods[26]. ZnO are the most attractive among the metallic oxide based green-synthesize nanomaterials due to its broad-spectrum antimicrobial action, UV absorption capabilities, photocatalytic potential, and relatively low toxicity[27]. In this context Plant-mediated ZnO NPs represent a sustainable and effective nanomaterial platform with strong biomedical and environment relevance. Phytochemicals in plant extracts act as reducing and stabilising agents, enabling controlled formation with biocompatibility, improved stability[28].

Therefore, the present study introduces a tri-component composite system composed of ZnO, *H. javanica*, and CS, designed to utilize the

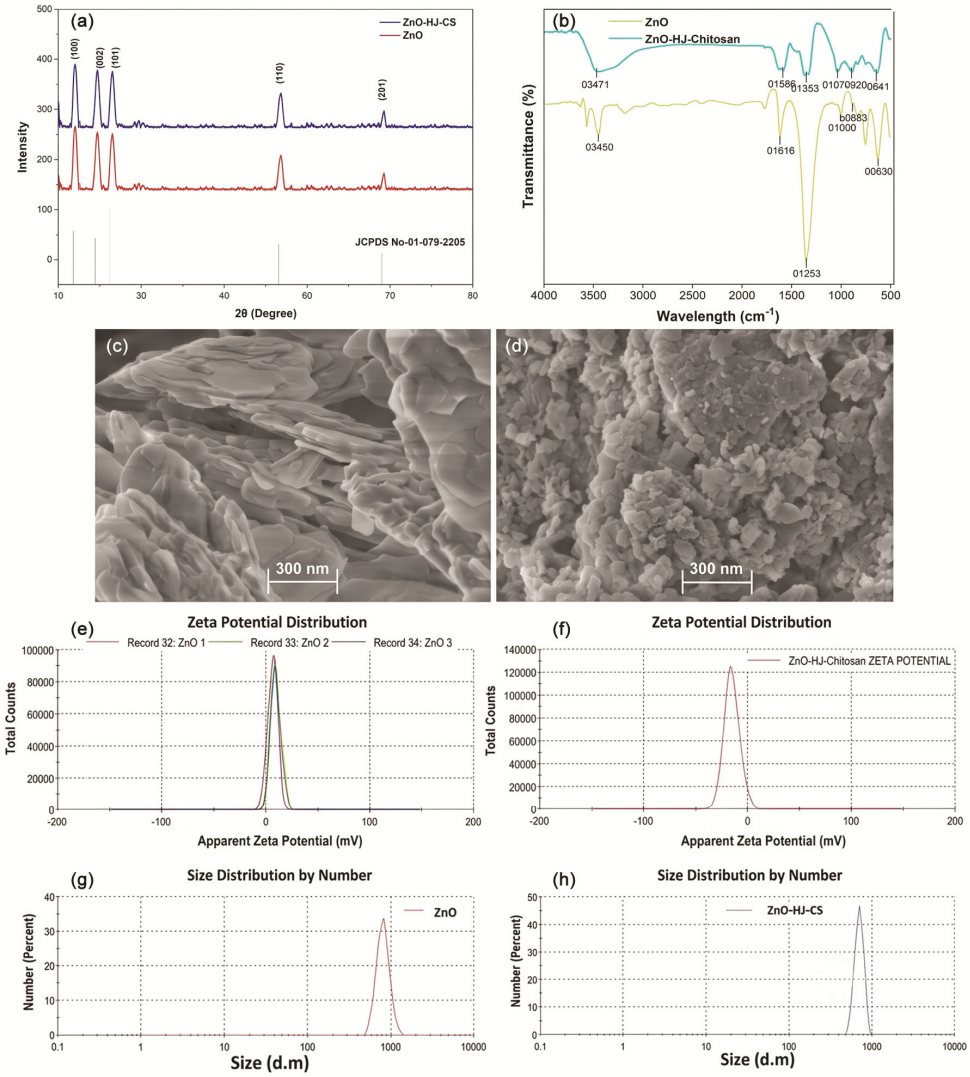


Fig. 1 — Comprehensive Characterisation of ZnO-HJ-CS composite. (A) X-ray diffraction (XRD) pattern showing sharp peaks at 2θ values corresponding to (100), (002), (101), (110), and (201) planes of hexagonal ZnO structure, confirming high crystallinity and phase purity based on JCPDS No. 01-079-2205; (B) FTIR spectra of pure ZnO and ZnO-HJ-CS composite indicating characteristic Zn-O str*et*ching (below 1000 cm^{-1}) and additional bands corresponding to hydroxyl, carbonyl, and aromatic functionalities introduced by *H. javanica* and chitosan; (C) SEM image of pure ZnO NPs showing uniform hexagonal plate–like morphology with smooth surface and minimal aggregation; (D) SEM image of ZnO-HJ-CS composite displaying rough, granular, and irregular morphology due to surface coating with biomolecules from plant extract and chitosan; (E & F) Zeta potential distribution showing a peak at –15.1 mV, indicating moderate colloidal stability of the composite in suspension; (G & H) PSD curve exhibiting a dominant peak at 702 nm and minor peaks at larger sizes, confirming nanoscale dimensions with partial agglomeration from surface modifications

Table 5 — Functional groups detected in ZnO-HJ-CS composite.

Functional groups	FTIR absorption Wave number (cm^{-1})	
	ZnO	ZnO-HJ-CS
O-H Str*et*ching	3450	3471
C=C str*et*ching	1616	1586
C-H str*et*ching	1353	1353
C-O str*et*ching	1000	1038
C=O str*et*ching	883	892
Zn-O str*et*ching	630	641

Complementary properties of each constituent for enhanced antibacterial and antioxidant properties.

XRD is a commonly used technique for characterising nanoparticles which is used to determine the composition of the particles by comparing the peak positions and intensities with reference patterns [29]. Accordingly, in our study the XRD of the ZnO-HJ-CS composite showed diffraction peaks corresponding to the hexagonal wurtzite structure of ZnO matched with the standard

Table 6 — Zeta potential values of pure ZnO and ZnO-HJ-CS composite.

S. no	Measurement	Value	Peaks	Mean (mV)	Area (%)	St Dev (mV)
			ZnO			
1	Zeta potential (mV)	15.0	Peak 1	15.1	100.0	7.62
2	Zeta Deviation (mV)		Peak 2	0.00	0.0	0.00
3	Conductivity (mS/cm)		Peak 3	0.00	0.0	0.00
			ZnO-HJ-CS			
1	Zeta potential (mV)	–15.1	Peak 1	–15.1	100.0	7.61
2	Zeta Deviation (mV)	7.53	Peak 2	0.00	0.0	0.00
3	Conductivity (mS/cm)	0.149	Peak 3	0.00	0.0	0.00

Table 7 — PSD peaks of pure ZnO and ZnO-HJ-CS composite measured via DLS.

S. no	Peaks	Size (d. nm)	% Number	PDI
		ZnO		
1	Peak 1	820.2	100	0.048
2	Peak 2	0.00	0.00	
3	Peak 3	0.00	0.00	
		ZnO-HJ-CS		
1	Peak 1	702.3	100	0.86
2	Peak 2	0.00	0.00	
3	Peak 3	0.00	0.00	

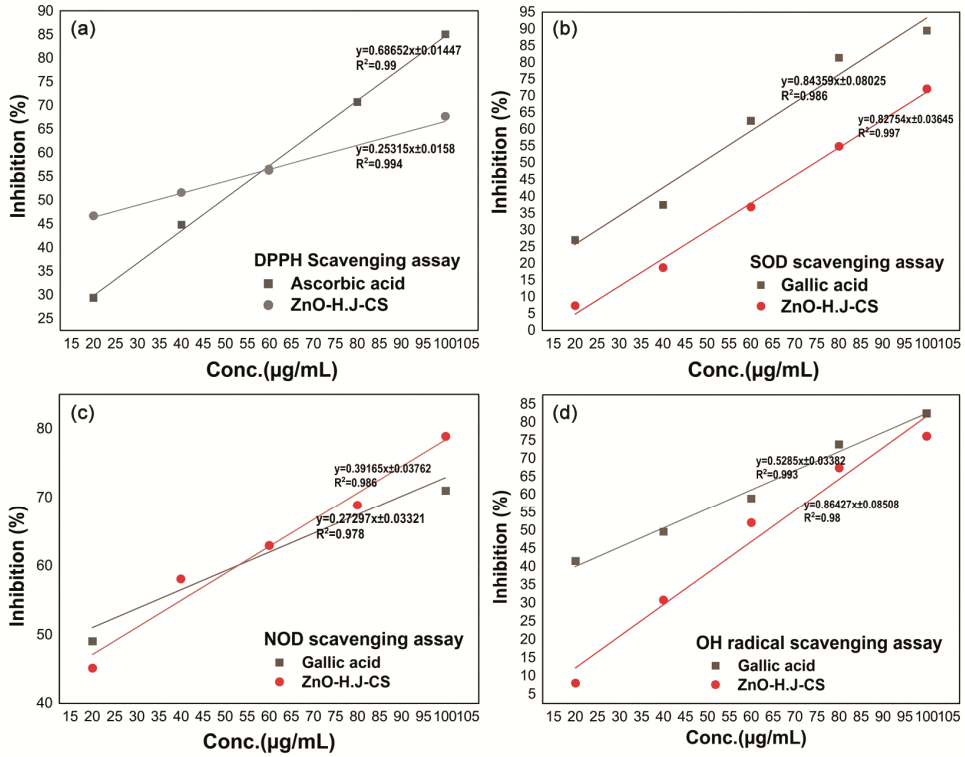


Fig. 2 — Antioxidant efficacy of ZnO-HJ-CS composite evaluated through *in vitro* radical scavenging assays. (A) DPPH radical scavenging assay: Demonstrates the ability of ZnO-HJ-CS and Ascorbic acid to scavenge stable DPPH free radicals. A dose–dependent increase in % inhibition is observed, with Ascorbic acid showing higher activity, (B) Nitric Oxide (NOD) scavenging assay: Compares the radical inhibition of ZnO-HJ-CS to Gallic acid against NO radicals generated in vitro. ZnO-HJ-CS exhibited moderate scavenging potential, (C) Superoxide Dismutase (SOD) scavenging assay: Shows the scavenging of superoxide radicals by ZnO-HJ-CS in comparison to Gallic acid, (D) Hydroxyl (OH) radical scavenging assay: Evaluates hydroxyl radical inhibition ability. ZnO-HJ-CS shows consistent activity, albeit lower than Gallic acid, indicating partial efficacy in neutralizing highly reactive OH radicals. Axes description: X–axis: Concentration of ZnO-HJ-CS composite (µg/mL); Y–axis: Percentage inhibition of the respective free radicals. Symbol Key: Black squares – Standard antioxidants (Ascorbic acid for DPPH, Gallic acid for NOD, SOD, OH assays), Red circles – Test sample: ZnO-HJ-CS composite

Table 8 — Antioxidant efficacy of ZnO-HJ-CS composite in comparison with standard antioxidants. IC_{50} represents the concentration at which 50% inhibition of free radicals is achieved. [All values are presented in mean ± standard deviation (SD)]

S. No	Antioxidant parameters	IC50		
		Standard	ZnO–HJ–CS	
1	DPPH	Ascorbic acid	10.2 ± 0.008	34.3 ± 0.0031
2	SOD	Gallic acid	42.6 ± 0.02	74.5 ± 0.03
3	NOD	Gallic acid	16.12 ± 0.03	27.3 ± 0.04
4	OH	Gallic acid	38.7 ± 0.02	63.6 ± 0.03

Table 9 — IC50 and the percentage inhibition of MEHJ on various bacterial strains after 24 and 48 h of treatment. [All values are presented in mean ± standard deviation (SD)].

Bacterial Strains	24h % Inhibition	24h IC_{50} (µg/mL)	48h % Inhibition	48h IC_{50} (µg/mL)
E. coli	48.40%	61.4 ± 0.04	47.13%	57.03 ± 0.03
S. aureus	45.60%	77.8 ± 0.045	42.30%	67.2 ± 0.035
S. pneumoniae	38.43%	63.9 ± 0.03	37.80%	44.41 ± 0.04
S. epidermidis	44.70%	68.5 ± 0.05	38.30%	72.2 ± 0.03
B. subtilis	33.43%	95 ± 0.04	28.80%	99.2 ± 0.03

Table 10 — MIC of MEHJ against tested bacterial strains. 80 µg/mL exhibited as MIC for *E. coli*, *S. epidermidis*, S. *pneumoniae* and *S. aureus* at 24 h incubation, whereas MIC after extension of incubation h till 48 h was 100 µg/mL for *S. epidermidis* and *S. pneumoniae*

Bacterial strains	MIC	
	24 h	48 h
E. coli	80 µg/mL	80 µg/mL
S. epidermidis	80 µg/mL	100 µg/mL
S. pneumoniae	80 µg/mL	100 µg/mL
S. aureus	80 µg/mL	80 µg/mL
B. subtilis	100 µg/mL	-

Table 11 — IC_{50} and percentage inhibition of ZnO-HJ-CS composite after 24 and 48 h. [All values are presented in mean ± standard deviation (SD)]

Bacterial Strains	24h % Inhibition	24h IC_{50} (µg/mL)	48h % Inhibition	48h IC_{50} (µg/mL)
E. coli	67.10%	53.7 ± 0.035	64.71%	53.31 ± 0.05
S. epidermidis	47.47%	71.8 ± 0.026	44.70%	73.8 ± 0.4
S. pneumoniae	45.00%	73.4 ± 0.02	44.25%	75.23 ± 0.033
S. aureus	67.17%	49.81 ± 0.09	62.30%	57.52 ± 0.04
B. subtilis	37.30%	87.1 ± 0.03	34.90%	85.09 ± 0.04

JCPDS reference, indicating successful formation of the crystalline ZnO phase within the composite.

This is further supported by FTIR spectra, which revealed ZnO-HJ-CS composite's characteristic Zn-O str*etc*hing bands, and broadening of peaks around OH, NH, amide and C-O/C-O-C bands together with Zn-O str*etc*hing indicate interaction between chitosan, *H. javanica* and ZnO. This result aligns with K *et al*., (2023)[29] findings which demonstrated that the coating of plant extract with ZnO exhibited shift in peaks.

Table 12 — MIC of ZnO-HJ-CS composite against test bacterial strains. 40 µg/mL exhibited as MIC for *E. coli* and *S. aureus* at 24 h incubation, whereas MIC after extension of incubation h till 48 h was 60 µg/mL

Bacterial strains	MIC	
	24 h	48 h
E. coli	40 µg/mL	60 µg/mL
S. epidermidis	80 µg/mL	100 µg/mL
S. pneumoniae	60 µg/mL	80 µg/mL
S. aureus	40 µg/mL	80 µg/mL
B. subtilis	80 µg/mL	100 µg/mL

Morphological evidence of ZnO-HJ-CS composite was obtained from SEM analysis, which revealed morphological transitions from smooth hexagonal ZnO structures to irregular, roughened surfaces upon modification with *H. javanica* and chitosan, suggesting surface functionalisation. Altınsoy *et al*., (2026) explained that ZnO surface and morphology changes upon coating, where morphology transitions from smooth homogeneous coatings to agglomerate [30].

Furthermore, the shift in the PSD of ZnO from 820 nm to 702 nm in ZnO-HJ-CS, along with the shift in zeta potential of ZnO-HJ-CS towards negative (-15 mV) indicates evidence of surface modification. Therefore, these findings provide consistent evidence for the effective coating of ZnO onto the composite framework.

Functionally, ZnO-HJ-CS composite demonstrated notable antioxidant activity, attributable to the redox-active phenolics and ROS-interacting properties of ZnO, along with chitosan's stabilization potential. Such antioxidant-loaded nanomaterials are increasingly relevant for biomedical applications, including wound healing and management of oxidative stress-related pathologies[31].

Comparatively, ZnO-HJ-CS composite demonstrated higher inhibitory effect against *E. coli* and *S. aureus*, this enhancement of antibacterial activity of ZnO-HJ-CS composite is attributed to mechanism of ZnO NPs generate reactive oxygen species, which damage bacterial membranes, proteins and DNA[32]. Additionally, the presence of chitosan is particularly beneficial in this context, as its cationic nature facilitates strong interactions with the anionic bacterial membrane components, enhancing permeability and leading to microbial cell lysis[33]. Similar studied by Agarwal *et al*., 2020, demonstrated that green synthesis resulted in enhanced antibacterial properties[26].

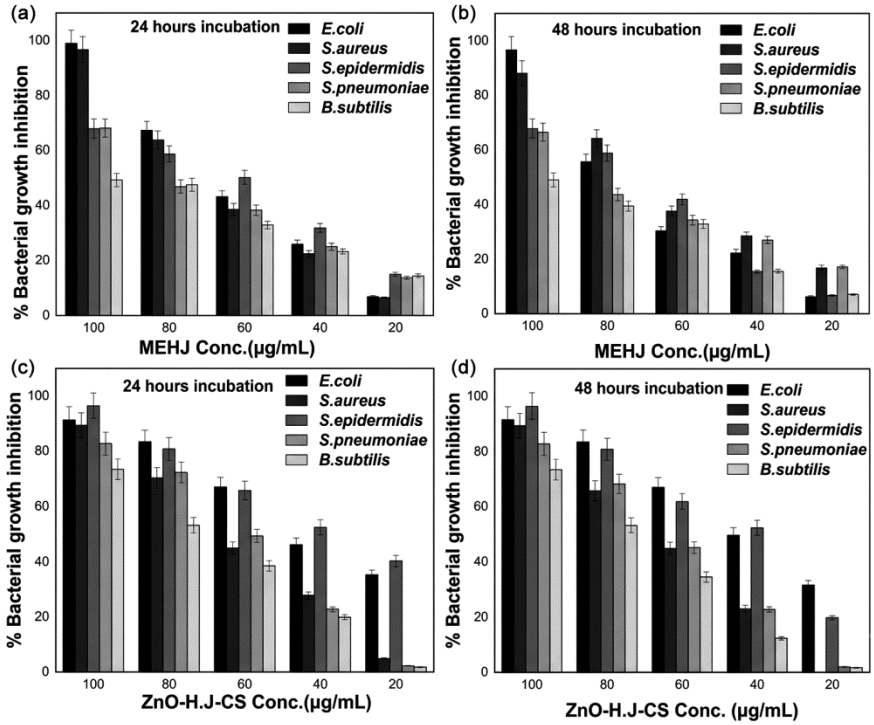


Fig. 3 — Comparative antibacterial activity of MEHJ extract and ZnO-HJ-CS composite against selected bacterial strains. (A–B) Bar graphs showing percentage inhibition of bacterial growth by MEHJ at different concentrations (20-100 µg/mL) after 24 h and 48 h of incubation. The inhibition is dose–dependent, with slightly improved efficacy after extended incubation, (C–D) Bar graphs depicting bacterial growth inhibition by ZnO-HJ-CS composite at concentrations ranging from 20-100 µg/mL after 24 h and 48 h

Table 13 — Zone of inhibition of ZnO-HJ-CS composite against tested bacterial strains at varying concentrations. Zone of inhibition was calculated using ImageJ application

	ZnO-HJ-CS composite		
S. No	Bacterial strains	Concentration (µg/mL)	Zone of inhibition
1	Control		52 mm
	E. coli	100 µg/mL	24 mm
		80 µg/mL	23 mm
		60 µg/mL	19.026 mm
		40 µg/mL	14.142 mm
2	Control		152 mm
	S. aureus	100 µg/mL	107.6 mm
		80 µg/mL	39.6 mm
		60 µg/mL	28 mm
		40 µg/mL	20.8 mm
3	Control		15 mm
	S. pneumoniae	100 µg/mL	12 mm
		80 µg/mL	6.325 mm
4	Control		15.524 mm
	B. subtilis	100 µg/mL	6.727 mm
		80 µg/mL	6.083 mm
5	Control		5.4 mm
	S. epidermidis	100 µg/mL	4. 1 mm
		80 µg/mL	3.6 mm

This study has also shed light on the nutritional and elemental composition of *H. javanica*, which demonstrated *H. javanica* as an important dietary source of carbohydrates fiber, and key minerals such as potassium, calcium, iron, magnesium, manganese and copper with notably low levels of toxic metals. The findings on high carbohydrate content not only supports its ethnobotanical role in traditional diets but also suggests its utility in green nanoparticle synthesis, particularly due to the abundance of hydroxyl-rich polysaccharides that can serve as effective reducing and stabilizing agents[34]. The fiber content, quantified at 14.12 g/100 g, is relatively high and indicative of the presence of non-digestible plant polysaccharides such as cellulose and lignin. From a nanotechnological standpoint, this fibrous matrix may aid in nanoparticle dispersion by contributing to steric stabilization[35]. Proteins and lipophilic compounds, despite their lower concentrations, may influence nanoparticle surface chemistry by providing functional groups that assist in surface capping and stabilization.

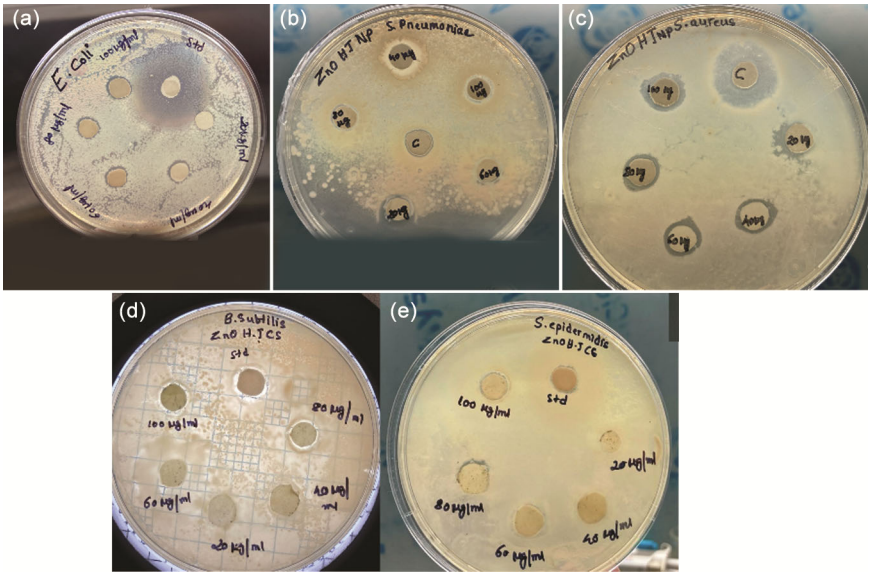


Fig. 4 — Zone of inhibition exhibited by ZnO-HJ-CS composite against (A) *E. coli* (B) *S. pneumoniae*, (C) *S. aureus*, (D) *B. subtilis*, and (E) *S. epidermidis*

Conclusion

The present study demonstrated the formulation of tri-component composite of ZnO with *H. javanica* and chitosan. The composite was characterized using XRD, FTIR, SEM, zeta potential and PSD analysis, which confirmed the formation of a coating of *H. javanica* and Chitosan on the surface of ZnO. The composite exhibited antioxidant activity and stronger antibacterial activity at a minimum concentration of 40 µg/ mL. Thus, synthesis of the composite using a medicinal plant can have useful medicinal applications in the treatment of bacterial infections. However, further studies will be required to validate the mechanism of action to support exploration for cytotoxicity, biocompatibility test, therapeutic, wound healing, and drug delivery applications.

Acknowledgement

All authors participated in the study's design and conceptualization. They have reviewed and approved the final manuscript.

Conflicts of interest

Both the authors declare no conflicts of interest.

References

1 Ettadili FE, Aghris S, Laghrib F, Farahi A, Saqrane S, Bakasse M, Lahrich S & Mhammedi MA El, Recent advances in the nanoparticles synthesis using plant extract: Applications and future recommendations. *J Mol Struct*, 1248 (2022) 131538.

2 Adeyemi JO, Oriola AO, Onwudiwe DC & Oyedeji AO, Plant extracts mediated metal–based nanoparticles: Synthesis and biological applications. *Biomolecules*, 12 (2022) 627.

3 Mouhaned Y, Sattar S & Ibrahim MA, A review on plant extract mediated green synthesis of zinc oxide nanoparticles and their biomedical applications. *Results Chem*, 7 (2024) 101368.

4 Zulfiqar Z, Khan RRM, Summer M, Saeed Z, Pervaiz M, Rasheed S, Shehzad B, Kabir F & Ishaq S, Plant–mediated green synthesis of silver nanoparticles: synthesis, Characterisation, biological applications, and toxicological considerations: a review. *Biocatal Agric Biotechnol*, 57 (2024) 103121.

5 Namasivayam K, Karuppanan A, Habibulla AK & Rangasamy N, GC–MS Profiling of Ethnomedicinal Plant *Hydrocotyle Javanica* Thunb. *Orient J Chem*, 33 (2017) 2127.

6 Bellai A, Deka S, Tag H, Bhattacharya K & Hui PK, Integrated Pharmacognostic and Computational Analysis of *Hydrocotyle javanica* Thunb. Phytochemicals as a Potential HER2 Tyrosine Kinase Inhibitor in Breast Cancer. *Pept Sci*, 116 (2024) e24372.

7 Mandal M, Misra D, Ghosh NN & Mandal V, Physicochemical and elemental studies of *Hydrocotyle javanica* Thunb. for standardization as herbal drug. *Asian Pac J Trop Biomed*, 7 (2017) 979.

8 Mandal M, Misra D & Mandal V, Antioxidant and nutritional properties of *Hydrocotyle javanica* Thunb. In *Biotechnol Biol Sci*, (2019) 356.

9 Sivakumar V, Evanjaline M & Ananthi Ravichandrun M, Determination of *In Vitro* Antioxidant Activity of *Hydrocotyle Javanica* Thunb Whole Plant Extracts. *World J Pharm Res*, 6 (2017) 824.

10 Dutta P, Kumari A & Mahanta M, Chitosan nanoparticle: Synthesis, Characterisation, and use as plant health materials. In *Chitin–Chitosan – Isolation, Properties, and Applications*, (2022) IntechOpen.

11 Ingle PU, Shende SS, Shingote PR, Mishra SS, Sarda V, Wasule DL, Rajput VD, Minkina T, Rai M, Sushkova S, Mandzhieva S & Gade A, Chitosan nanoparticles (ChNPs):

A versatile growth promoter in modern agricultural production. *Heliyon*, 8 (2022) e11893.
12 Yu J Wang D, Geetha N, Khawar KM, Jogaiah S & Mujtaba M, Current trends and challenges in the synthesis and applications of chitosan–based composites for plants: A review. *Carbohydr Polym*, 261 (2021) 117904.
13 Ali SA, Ali ES, Hamdy G, Badawy MSEM, Ismail AR, El–Sabbagh IA, El–Fass MM & Elsawy MA, Enhancing physical characteristics and antibacterial efficacy of chitosan through investigation of microwave–assisted chemically formulated chitosan–coated ZnO and chitosan/ZnO physical composite. *Sci Rep*, 14 (2024) 9348.
14 Misra D, Mandal M, Nath Ghosh N & Mandal V, Pharmacognostic Standardization of an Ethnomedicinal Aquatic Herb, *Monochoria hastata* (L.) Solms for its Antibacterial Potentiality. *Pharmacogn J*, 10 (2018) 533.
15 Das A, Ringu T, Ghosh S & Pramanik N, Processing and biomedical applications of novel eco–sustainable fluconazole–loaded zinc oxide (ZnO) encapsulated chitosan (CS) biopolymer composite by inhibiting microbe species against candidiasis. *Mater Today Commun*, 37 (2023) 107071.
16 Mughal TA, Ali S, Mumtaz S, Summer M, Saleem MZ, Hassan A & Hameed MU, Evaluating the biological (antidiabetic) potential of TEM, FTIR, XRD, and UV–spectra observed berberis lyceum conjugated silver nanoparticles. *Microsc Res Tech*, 87 (2024) 1286.
17 Mehta BK, Chhajlani M & Shrivastava BD, Green synthesis of silver nanoparticles and their Characterisation by XRD. *J Phys Conf Ser*, 836 (2017) 012050.
18 Das C, Sen S, Singh T, Ghosh T, Paul SS, Kim TW, Jeon S, Maiti DK, Im J & Biswas G, Green synthesis, Characterisation and application of natural product coated magnetite nanoparticles for wastewater treatment. *Nanomaterials (Basel)*, 10 (2020) 1615.
19 Anandalakshmi K, Venugobal J & Ramasamy V, Characterisation of silver nanoparticles by green synthesis method using Pedalium murex leaf extract and their antibacterial activity. *Appl Nanosci*, 6 (2016) 399.
20 Mohamed AA, Sameeh MY & El–Beltagi HS, Preparation of seaweed nanopowder particles using planetary ball milling and their effects on some secondary metabolites in date palm (Phoenix dactylifera L.) seedlings. *Life (Basel)*, 12 (2022) 39.
21 Zamani M, Moradi DA & Jabbari M, Scavenging performance and antioxidant activity of γ–alumina nanoparticles towards DPPH free radical: Spectroscopic and DFT–D studies. *Spectrochim Acta A Mol Biomol Spectrosc*, 201 (2018) 288.
22 Ragab EM, El Gamal DM, Mohamed TM & Khamis AA, Impairment of electron transport chain and induction of apoptosis by chrysin nanoparticles targeting succinate–ubiquinone oxidoreductase in pancreatic and lung cancer cells. *Genes Nutr*, 18 (2023) 4.
23 Kavi RR, Hussein MZ, Fakurazi S, Yusoff K & Masarudin MJ, Increased ROS scavenging and antioxidant efficiency of Chlorogenic acid compound delivered *via* a chitosan nanoparticulate system for efficient *in vitro* visualization and accumulation in human renal adenocarcinoma cells. *Int J Mol Sci*, 20 (2019) 4667.
24 Ghaffar S, Abbas A, Naeem–Ul–Hassan M, Assad N, Sher M, Ullah S, Alhazmi HA, Najmi A, Zoghebi K, Al Bratty M, Hanbashi A, Makeen HA & Amin HMA, Improved photocatalytic and antioxidant activity of Olive fruit extract–mediated ZnO NPs. *Antioxidants (Basel)*, 12 (2023) 1201.
25 Bashal AH, Riyadh SM, Alharbi W, Alharbi KH, Farghaly TA & Khalil KD, Bio–Based (Chitosan–ZnO) Composite: Synthesis, Characterisation, and Its Use as Recyclable, Ecofriendly Biocatalyst for Synthesis of Thiazoles Tethered Azo Groups. *Polymers*, 14 (2022) 386.
26 Agarwal H, Menon S & Shanmugam VK, Functionalization of zinc oxide nanoparticles using Mucuna pruriens and its antibacterial activity. *Surf Interfaces*, 19 (2020), 100521.
27 Nandhini J, Karthikeyan E & Rajeshkumar S, Green synthesis of zinc oxide nanoparticles: Eco–friendly advancements for biomedical marvels. *Resour Chem Mater*, 3 (2024) 294.
28 Gare A, Bisal P, Ghosh S & Pramanik N, Green synthesis to biomedical applications: Zinc oxide nanoparticles in eco-friendly formulations. *Nanotechnol Environ Eng*, 11 (2026) 15.
29 Supi KK, Parvathy Namboothiri PM & Vasundhara M, Enhanced photocatalytic activity in ZnO NPs developed using novel Lepidagathis ananthapuramensis leaf extract. *RSC Adv*, 13 (2023) 1497.
30 Altınsoy Ş, Beköz Üllen N, Karabulut Şevk G & Karakuş S, Surface Roughness-Dependent Morphology and Corrosion Protection of Polymeric–Ceramic ZnO Nanocoatings on Ti6Al4V Alloys. *Coatings*, 16 (2026) 823.
31 Madhan G, Begam AA, Varsha LV, Ranjithkumar R & Bharathi D, Facile synthesis and Characterisation of chitosan/zinc oxide composite for enhanced antibacterial and photocatalytic activity. *Int J Biol Macromol*, 190 (2021) 259.
32 Khajuria AK, Kandwal A, Sharma RK, Bachheti RK, Worku LA & Bachheti A, *In vitro* antioxidant and antibacterial activities of biogenic synthesized zinc oxide nanoparticles using leaf extract of Mallotus philippinensis Mull. *Arg. Sci Rep*, 15 (2025) 6541.
33 Ali AM, Hamed AM, Taher MA, Abdallah MH, Abdel–Motaleb M, Ziora ZM & Omer AM, Fabrication of Antibacterial and Antioxidant ZnO–Impregnated Amine–Functionalized Chitosan Bio–Composite Membrane for Advanced Biomedical Applications. *Molecules*, 28 (2023) 7034.
34 Zhang R, Liu X, Zhang W, Cui B, Du Y, Huang Y, Li W, Liu Q, Ren C & Tang Z, A review of polysaccharide–based hydrogels: From structural modification to biomedical applications. *Int J Biol Macromol*, 310 (2025) 143519.
35 Swierczewska M, Han HS, Kim K, Park JH & Lee S, Polysaccharide-based nanoparticles for theranostic nanomedicine. *Adv Drug Deliv Rev*, 99 (2016) 70.